Synthesis and Characterization of Iodinated Tetrahydroquinolines Targeting the G Protein-Coupled Estrogen Receptor GPR30

Chinnasamy Ramesh,[†] Tapan K. Nayak,[‡,ǁ] Ritwik Burai,[†] Megan K. Dennis,[‡] Helen J. Hathaway,[‡,§] Larry A. Sklar,[§,⊥] Eric R. Prossnitz,[‡,§] and Jeffrey B. Arterburn*[,†,§]

[†]*Department of Chemistry and Biochemistry, New Mexico State University, Las Cruces, New Mexico 88003,* [‡]*Department of Cell Biology and Physiology, School of Medicine, University of New Mexico Health Science Center, Albuquerque, New Mexico 87131,* [§]*UNM Cancer Center, University of New Mexico Health Science Center, Albuquerque, New Mexico 87131,* [ǁ]*College of Pharmacy, University of New Mexico Health Science Center, Albuquerque, New Mexico 87131, and* [⊥]*Department of Pathology, School of Medicine, University of New Mexico Health Science Center, Albuquerque, New Mexico 87131*

A series of iodo-substituted tetrahydro-3*H*-cyclopenta[*c*]quinolines was synthesized as potential targeted imaging agents for the G protein-coupled estrogen receptor GPR30. The affinity and specificity of binding to GPR30 versus the classical estrogen receptors ERα/β and functional responses associated with ligand-binding were determined. Selected iodo-substituted tetrahydro-3*H*-cyclopenta[*c*]quinolines exhibited IC$_{50}$ values lower than 20 nM in competitive binding studies with GPR30-expressing human endometrial cancer cells. These compounds functioned as antagonists of GPR30 and blocked estrogen-induced PI3K activation and calcium mobilization. The tributylstannyl precursors of selected compounds were radiolabeled with ^{125}I using the iodogen method. In vivo biodistribution studies in female ovariectomized athymic (NCr) nu/nu mice bearing GPR30-expressing human endometrial tumors revealed GPR30-mediated uptake of the radiotracer ligands in tumor, adrenal, and reproductive organs. Biodistribution and quantitative SPECT/CT studies revealed structurally related differences in the pharmacokinetic profiles, target tissue uptake, and metabolism of the radiolabeled compounds as well as differences in susceptibility to deiodination. The high lipophilicity of the compounds adversely affects the in vivo biodistribution and clearance of these radioligands and suggests that further optimization of this parameter may lead to improved targeting characteristics.

Introduction

Estrogen is a critical hormone that regulates a multitude of biological processes. The nuclear estrogen hormone receptors (ERα and ERβ)[a] are best characterized for their regulation of gene expression and consequently are important targets in many disease states that include cancer, skeletal, neurological, and immunological conditions. New evidence of estrogen's role in nongenomic signal transduction pathways has expanded the classical paradigm of hormone function and suggests corresponding significance for mammalian biology.[1,2] The discovery of the G protein-coupled estrogen receptor GPR30 (IUPHAR designation: GPER), a seven transmembrane GPCR, has introduced an entirely new class of receptor to the milieu of nongenomic and genomic estrogen-mediated signaling.[3–6] Significant overlap exists between the cellular and physiological aspects of GPR30 function and that of the classical estrogen receptors,[7] as well as in their ligand specificity and pharmacological profiles.[8] Studies with breast,

ovarian, and endometrial cancers indicate roles for both ERα/β and GPR30 in tumoregenesis and suggest the potential for clinical diagnostic and prognostic applications based on receptor expression.[9,10] The development of drugs that are capable of differentiating the pharmacology of classical estrogen receptors, which have different tissue distribution profiles and distinct patterns of gene regulation, by selectively modulating the activity of the individual receptor subtypes ERα/β is widely recognized as an important strategy for obtaining improved therapeutics.[11,12] Unraveling the pharmacological profiles and specificities of these three estrogen receptors will contribute toward understanding the interrelated physiological roles of each receptor and facilitate the development of the next generation of receptor-specific drugs.

We combined virtual and biomolecular screening to identify the first GPR30-selective agonist 1-[4-(6-bromo-benzo[1,3]dioxol-5-yl)-3a,4,5,9b-tetrahydro-3*H*-cyclopenta-[*c*]quinolin-8-yl]ethanone (**G-1**, **1**, Figure 1).[13] This compound has found application as a molecular probe for in vitro and in vivo characterization of GPR30-mediated effects.[14–25] A focused effort including synthetic chemistry and virtual and biomolecular screening through the New Mexico Molecular Libraries Screening Center recently provided the complementary GPR30-selective antagonist 4-(6-bromo-benzo[1,3]dioxol-5-yl)-3a,4,5,9b-tetrahydro-3*H*-cyclopenta[*c*]quinoline (**G-15**, **2**, Figure 1).[26] This compound is capable of blocking cellular
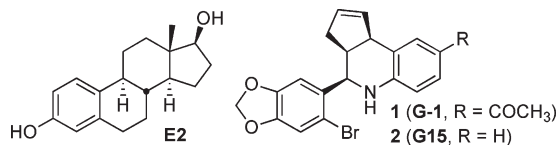

Figure 1. Structures of 17β-estradiol (**E2**), GPR30-selective agonist (**G-1**), and antagonist (**G15**).

activation by estrogen in cells expressing GPR30 but has no effect on estrogen-stimulated intracellular calcium mobilization or nuclear accumulation of PIP3 induced through ERα or ERβ. The intriguing pair of compounds, which share the tetrahydro-3*H*-cyclopenta[*c*]quinoline scaffold, have the potential to further investigations of fundamental questions regarding GPR30 physiology, including assessment of potential clinical roles for this receptor in disease progression and therapeutic response.

There remain significant opportunities for further delineating the individual biological roles of these estrogen receptors through the application of radiolabeled GPR30-selective ligands. The commercial availability of [^{3}H]-17β-estradiol has facilitated the characterization of receptor distribution and ligand binding of the classical estrogen receptors using cellular extracts, cell culture, and in vivo models. The development of estrogen receptor ligands radiolabeled with positron- or γ-emitting halogen isotopes for PET and SPECT imaging applications, as well as potential therapeutic applications based on estrogen receptor targeting, has been intensively studied over the past 30 years.[27−31] Clinical oncologists have successfully used [^{18}F]FES for staging and visualizing primary and metastatic carcinomas.[32,33] The quantification of ERα and ERβ levels affords predictive value for determining outcomes of hormone therapy in breast cancer.[34,35] The development of radiolabeled 17α-iodovinylestradiols has progressed to clinical assessment of [^{123}I]-labeled 11β-methoxyiodovinylestradiol for estrogen receptor imaging in breast cancer.[36] Radiolabeled analogues incorporating Auger-emitting isotopes [^{125}I] and [^{123}I] have potential as therapeutic agents for estrogen receptor expressing tumors.[30,37] The high specific activity and sensitivity of detection possible using the γ-emitting isotope [^{125}I] offer practical advantages for receptor binding studies in the laboratory and allow efficient determination of receptor content in tissues and convenient detection and quantification of images. The development of GPR30-selective radiotracers would have significant value for characterizing receptor binding properties and investigations of imaging applications based on targeting this receptor. The desired performance characteristics of these agents should include high selectivity for GPR30, low affinity for ERα/β, effective receptor-mediated uptake, and retention accompanied by rapid clearance from nontarget tissue and organs in order to provide images that directly correspond to GPR30 expression levels with minimum background detection levels.

Herein, we report the synthesis of a series of iodo-substituted quinoline derivatives **3**−**9** as selective ligands and potential targeted imaging agents for GPR30 that meet some of the performance characteristics outlined above. These compounds were evaluated against a panel of functional and competitive ligand binding assays using GPR30 and ERα/β transfected COS7 as well as Hec50 and SKBr3 cells, which endogenously express only GPR30, to evaluate receptor selectivity and potential cross-reactivity. Selected derivatives **8** and **9** were demonstrated to be GPR30-selective
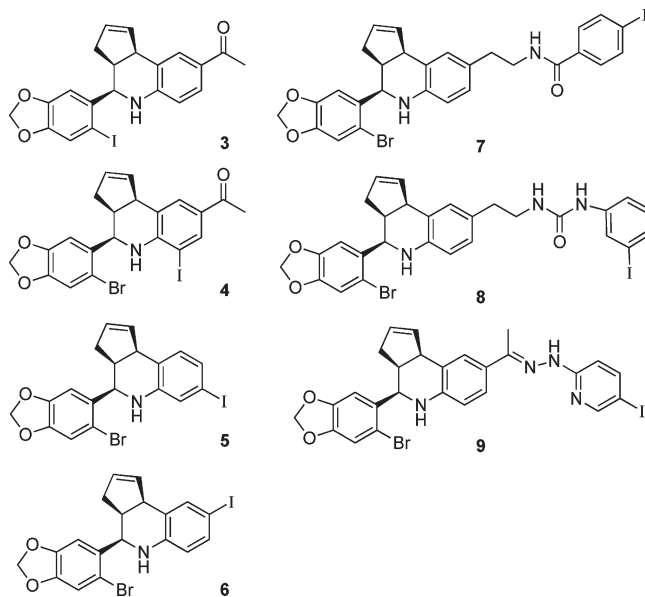

Figure 2. Structure of direct and pendent iodo-substituted tetrahydro-3*H*-cyclopenta[*c*]quinoline derivatives.

antagonists. The corresponding tributylstannane derivatives were radiolabeled with [^{125}I] and used to determine GPR30 receptor binding affinity in cell culture and to evaluate biodistribution and in vivo imaging in a mouse tumor model.

Results and Discussion

Synthetic Chemistry. We designed a focused series of iodinated analogues using structure−activity considerations obtained during our development of the GPR30-selective agonist and antagonist compounds **1** and **2** (Figure 1).[13,26] The compounds illustrated in Figure 2 possess either direct halogenation of the aryltetrahydro-3*H*-cyclopenta[*c*]quinoline scaffold (**3**−**6**) or conjugation of an iodinated appendage (**7**−**9**). The iodinated analogue **3** of **1** was a promising candidate because of the relatively minor increase in steric volume resulting from iodide substitution. The positions 6−8 of the tetrahydrocyclopenta[*c*]quinoline scaffold were also identified as possible sites for introducing halogen substitutions. Series **4**−**6** have iodo substitutions at positions 6−8 of the 1,2,3,4-tetrahydroquinoline. The other derivatives (**7**, **8**) contain iodophenyl appendages connected at the C8 position with a flexible *N*-ethylcarboxamide or urea linkages, respectively. Hydrazone **9** was prepared directly from **1**.

The tetrahydro-3*H*-cyclopenta[*c*]quinoline scaffold is synthetically accessible using the three-component Povarov cyclization.[38] We evaluated a series of reaction conditions employing a variety of protic and Lewis acid catalysts in order to optimize reaction rate, yield, and diastereoselectivity for the construction of the compounds in this series. Our optimized procedure was based on the application of lanthanide salts as catalysts for the Povarov cyclization,[39] and we employed Sc(OTf)$_3$ in acetonitrile, which generally provided rapid reaction times, high product yield, and diastereoselective formation of the *syn*- or *endo*-products (Scheme 1). This approach provided a direct route for the preparation of the desired iodides **3**−**6**. In several cases the *endo* diastereomer ratio was further enriched by crystallization. All compounds used in biological studies were evaluated as racemic mixtures consisting of >95% *endo* diastereomer.

The synthesis of **4** from 1-(4-amino-3-iodophenyl)ethanone, 6-bromopiperonal, and cyclopentadiene was accomplished in moderate yield as illustrated in Scheme 1. This derivative possesses an iodide substituent at the 6-position of the tetrahydro-3*H*-cyclopenta[*c*]quinoline system and retains the ketone group of **1**. Monitoring the reaction revealed that both the intermediate imine formation and subsequent cyclization were slow in comparison with the other aniline substrates, attributed to increased steric hindrance of the *o*-iodide, and the yield was not improved by attempted cyclization of the preformed imine. The related iodinated compounds **5** and **6**
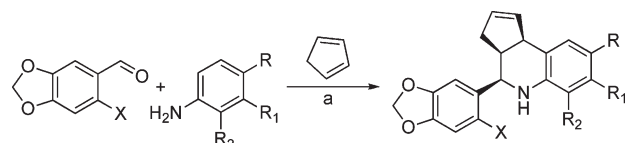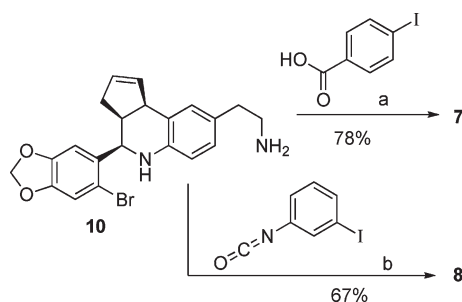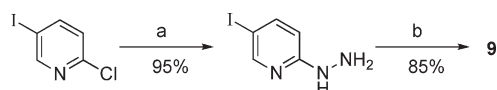
substituted at the 7- and 8-positions were prepared analogously from the corresponding *m*- or *p*-iodoanilines, respectively. The derivative **10**, possessing a pendant aminoethyl functional group, was prepared using *t*Boc-protected aminophenethylamine[45] and was isolated in 95% yield after deprotection with TFA/CH$_2$Cl$_2$. The amine **10** was coupled with *p*-iodobenzoic acid to provide benzamide **7** as shown in Scheme 2. The related urea **8** was prepared by coupling **10** with *m*-iodophenyl isocyanate (Scheme 2).

The synthesis of **9** required 5-iodopyridin-2-ylhydrazine,[40] which was prepared by substitution of commercially available 2-chloro-5-iodopyridine with hydrazine hydrate in pyridine as shown in Scheme 3. The desired hydrazone **9** was obtained by melting the hydrazine with **1** at 170−180 °C, followed by preparative reverse phase chromatography.

Assessment of the lipophilicity and solubility was an additional consideration for selecting possible imaging agents. The log $P_{o/w}$ values for the selected iodides **3**−**9** were calculated and tabulated in Table 1. All seven iodinated compounds exhibited increased lipophilicity relative to **1**. These log $P_{o/w}$ values paralleled the qualitative experimental observations of the solubility of the compounds. Compound **7** was poorly soluble in alcohols (MeOH and EtOH), halogenated organic solvents (CH$_2$Cl$_2$, CHCl$_3$), and acetonitrile but was soluble in DMSO with heating. The urea-linked derivative **8** exhibited a greater range of solubility, including alcoholic, halogenated solvents, acetonitrile, and DMF. The hydrazone **9** was soluble in a variety of protic and aprotic solvents.

With the iodinated compounds **3**−**9** in hand, we proceeded to synthesize the tributyltin-substituted analogues in preparation for radiolabeling experiments.[41] The accessibility of the corresponding stannane and efficiency of subsequent iodine exchange combined with analysis of receptor binding and activation properties (vida infra) were factors considered for the selection of compounds that were advanced for radiolabeling experiments and in vivo imaging studies. Compound **3** is a close structural analogue of **1**; however, attempts to prepare the corresponding stannane **12** directly by palladium-catalyzed exchange of **1** or **3** with hexabutyldistannane were unsuccessful (Scheme 4). The benzylic amine functionality is susceptible to cyclopalladation and likely results in catalyst degradation.[42] An alternative route

Scheme 1[a]

a Reagents: Sc(OTf)$_3$, CH$_3$CN, 23 °C, 2−5 h.

Scheme 2[a]

a Reagents: (a) PyBOP, *i*PrNEt$_2$, DMF; (b) Et$_3$N, DMF.

Scheme 3[a]

a Reagents: (a) H$_2$NNH$_2$, H$_2$O, pyridine, 120 °C, 5 h; (b) **1**, 170−180 °C melt.

Table 1. Binding and Functional Characterization of GPR30-Targeted Compounds

compd	CLogP	ERα binding[a]	ERβ binding[a]	GPR30 binding, IC$_{50}$ (nM)	GPR30 agonism (calcium)[b]	GPR30 antagonism (calcium)[c]	ERα agonism (PI3K)[d]	ERα antagonism (PI3K)[e]	GPR30 agonism (PI3K)[d]	GPR30 antagonism (PI3K)[e]
E2	3.37	+++	+++	3−6	+++	−	+++	−	+++	−
1	4.55	−	−	7	+++	−	−	−	+++	−
3	4.94	−	−	ND	+++	+/−	−	−	+++	−
4	5.82	−	+/−	ND	−	+	−	−	+/−	+/−
5	6.00	−	−	ND	+	+/−	−	−	+/−	−
6	6.00	−	+/−	1.7	+	+/−	−	−	−	−
7	6.71	−	+/−	16.2	+	+/−	−	−	++	+/−
8	7.00	−	−	8.4	−	++	−	−	−	+++
9	6.35	+/−	−	1.7	−	+	−	−	−	+

[a] +/− denotes that 10 μM compound blocks ∼25% of 10 nM E2-Alexa binding. − denotes <10% inhibition of E2 binding. [b] +++ denotes that calcium mobilization in response to 10 μM compound is 80−100% of reference compound (200 nM E2). + denotes that calcium mobilization in response to 10 μM compound is 20−40% of reference compound. [c] ++ denotes that 10 μM compound blocks 80−100% of 200 nM E2-induced calcium mobilization. + denotes that 10 μM compound blocks 50−60% of E2-induced calcium mobilization. +/− denotes that 10 μM compound blocks less than 50% of E2-induced calcium mobilization. [d] +++ denotes activation of PI3K similar by 10 μM compound similar to activation induced by 10 nM reference compound (E2). ++ and +/− denote decreased activation of PI3K (qualitative assay). [e] +++ denotes complete antagonism of 10 nM E2-induced PI3K activation by 10 μM compound. + and +/− denote lesser degrees of antagonism of 10 nM E2-mediated PI3K activation by 10 μM compound.
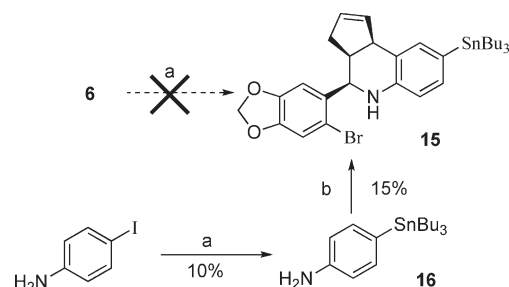
Scheme 4[a]
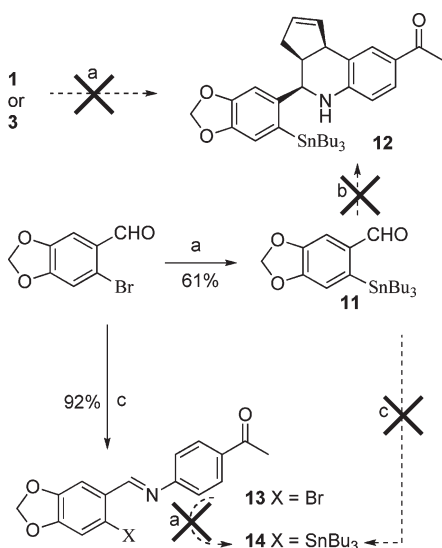
[a] Reagents: (a) $(SnBu_3)_2$, $Pd(PPh_3)_4$, dioxane, 100 °C; (b) $Sc(OTf)_3$, CH_3CN, cyclopentadiene, 4-aminoacetophenone; (c) 4-aminoacetophenone, 170−180 °C melt.

to **12** was attempted using the $SnBu_3$-substituted piperonal **11**, prepared from 6-bromopiperonal by Pd-catalyzed stannylation; however, the cyclization of **11** was unsuccessful using either our optimized procedure or various other protic and Lewis acid catalysts. Attempts to form the intermediate imine **14** under a variety of forcing conditions were also unsuccessful, resulting in unreacted **11** and aminoacetophenone. The failure to form imine **14** contrasts with the facile formation of the brominated analogue **13** and can be attributed to the increased steric demands of the stannyl group of **11** in comparison with 6-bromopiperonal. Attempted stannylation of brominated imine **13** to form **14** was also unsuccessful.

While the direct Pd-catalyzed tributylstannylation of iodides **4**−**9** appears feasible, in practice we were unable to effect this transformation because of the competing reactivity of the 6-bromobenzo[1,3]dioxol-5-yl discussed previously. The attempted stannylation of **6** to obtain **15** was unsuccessful; therefore, an alternative stepwise approach was investigated as shown in Scheme 5. The Pd-catalyzed exchange of 4-iodoaniline with $(SnBu_3)_2$ to produce **16** required extended reaction times and heating and proceeded in low yield (~10%) accompanied by unreacted starting material under these conditions, presumably due to increased electron density from the *p*-amine substituent. The attempted cyclization of **16** under a variety of conditions resulted in poor yields of **15**, and significant amounts of the proto-dehalogenated material were observed. Preliminary initial iodination experiments of **15** with iodogen demonstrated poor incorporation of iodide and proteodestannylation as the primary competing reaction. The poor preparative yield of tributylstannane **15** and the subsequent inefficient iodination of this derivative were recognized as significant disadvantages for a putative imaging agent. In contrast, the three-component cyclization of the *m*-tributylstannylaniline **17** proceeded efficiently to provide **18** (Scheme 6). This result confirms the positional dependence of substitution on the aniline ring that was problematic for para-substituted analogue **16**.
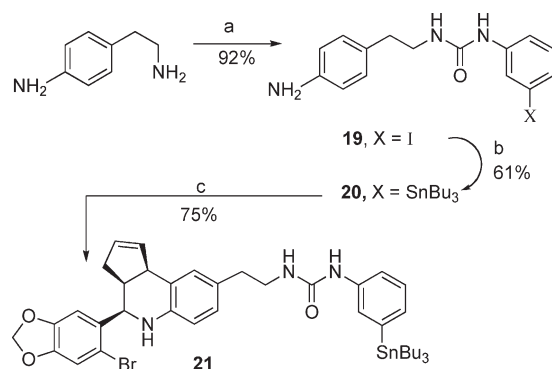
The primary aliphatic amine of 4-(2-aminoethyl)aniline reacted preferentially with *m*-iodophenyl isocyanate to give

Scheme 5[a]

[a] Reagents: (a) $(SnBu_3)_2$, $Pd(PPh_3)_4$, dioxane, 100 °C, 16 h; (b) $Sc(OTf)_3$, CH_3CN, 6-bromopiperonal.

Scheme 6[a]
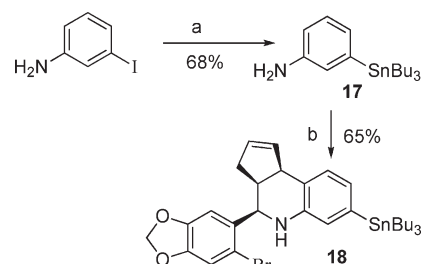
[a] Reagents: (a) $(SnBu_3)_2$, $Pd(PPh_3)_4$, dioxane, 100 °C, 15 h; (b) $Sc(OTf)_3$, CH_3CN, 6-bromopiperonal, 2 h.

Scheme 7[a]

[a] Reagents: (a) 3-iodophenyl isocyanate, CH_2Cl_2; (b) $(SnBu_3)_2$, Pd-$(PPh_3)_4$, dioxane, 100 °C; (c) $Sc(OTf)_3$, CH_3CN, 6-bromopiperonal.

the urea **19** (Scheme 7). Palladium catalyzed exchange with bis(tributyltin) gave the tributyltin derivative **20**. Scandium-(III) catalyzed cyclization of **20** with 6-bromopiperonal and cyclopentadiene gave the desired product **21** in good yield.

Stannylation of 2-chloro-5-iodopyridine provided an efficient route for the preparation of 2-chloro-5-(tributylstannyl)-pyridine. This compound was previously synthesized by halogen−metal exchange with *n*-butyllithium followed by stannylation with tributylstannyl chloride.[43] Nucleophilic substitution of chloride with hydrazine gave the desired 2-hydrazinyl-5-(tributylstannyl)pyridine (Scheme 8). Hydrazone formation with **1** occurred upon melting, and the resulting product **22** was purified by preparative reverse phase chromatography.

Receptor Binding and Functional Properties. The iodinated compounds **3**−**9** were evaluated in cell-based binding and functional assays to determine the potency and type of signaling response (agonism or antagonism) associated with

Scheme 8[a]
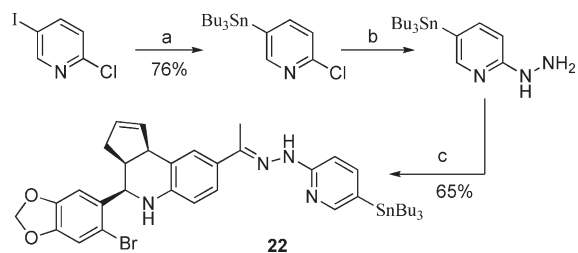
[a] Reagents: (a) (SnBu₃)₂, Pd(PPh₃)₄, dioxane, 100 °C; (b) H₂NNH₂, H₂O, pyridine, 120 °C, 24 h ; (c) **1**, 170−180 °C melt.

ligand-induced GPR30- and ERα/β-mediated signaling (summarized in Table 1 with numerical binding data provided in the Supporting Information). These compounds were profiled using transfected COS7 cells expressing GPR30, ERα, or ERβ, in addition to Hec50 and SKBr3 cells, which endogenously express only GPR30. Functional characterization of the compounds using either the extent (or inhibition of E2-mediated increase) in intracellular calcium or the activation of PI3K as measured by production of PIP3 in the nucleus is as previously described.[5,13,26] The specificity of the response in these assays was demonstrated in control COS7 cells that do not endogenously express GPR30 or ERα/β. The comparison of the observed ligand-induced responses across cells expressing individual receptors in comparison to estrogen-induced responses, in addition to comparison of differential binding to receptors, provides a profile of the selectivity/cross-reactivity of the compounds.

We have previously shown the specificity of binding of the GPR30-selective ligand **1** to GPR30 versus the classical estrogen receptors ERα/β using cell-based competitive binding assays.[13] In order to characterize the selectivity of iodinated compounds **3−9**, the same cell based assay employing transfected COS7 cells was used to evaluate binding of these compounds to the classical estrogen receptors. These assays confirmed that compounds **3**, **5**, and **8**, like **1**, do not exhibit binding to either of the classical estrogen receptors ERα/β. Compounds **4**, **6**, and **7** exhibited minimal binding to ERβ at high concentrations (blocking less than 35% of E2-Alexa633 binding when present at 10 μM). Hydrazone **9** was the only iodinated derivative to show any detectable binding to ERα, which was also minimal. These low levels of competition at 10 μM are compared to an IC₅₀ for estrogen in the same assay of approximately 0.4 nM.[13]

Cell-based functional assays for compounds **3−9** were carried out in parallel to binding studies in order to assess the functional characteristics of this series of compounds. Stimulation of cells expressing ERα or GPR30 results in the receptor-dependent activation of PI3K which can be visualized using the pleckstrin homology (PH)-domain of Akt fused to RFP (PH-RFP), which serves as a reporter of PIP3 localization. Receptor activation leads to the translocation of this reporter from a cytoplasmic or plasma membrane-associated localization to the nucleus.[5,13] We evaluated the ability of compounds **3−9** alone to induce PI3K activation or the ability of these compounds to block estrogen-stimulated PI3K activation to determine the agonist and antagonist properties of each compound in transfected COS7 cells expressing ERα or GPR30; additionally COS7 cells transfected with PH-RFP reporter alone were treated with all compounds to confirm that the results in receptor-transfected cells were receptor-dependent. As expected because of

their lack of binding to ERα, compounds **3−8** were unable to induce either activation of PI3K or inhibit estrogen-induced PI3K activation in ERα transfected COS7 cells. Compound **9**, which exhibited very weak binding to ERα, was also unable to influence PI3K activity in ERα transfected COS7 cells. Additionally, none of compounds **3−9** were able to activate PI3K in COS7 cells lacking estrogen receptor expression. Thus, none of the seven iodinated derivatives show any functional activity mediated through ERα or any ability to activate PI3K via other mechanisms. Compound **3** showed strong GPR30-dependent activation of PI3K as expected for an isostructural analogue of **1**. A regioisomeric dependence of iodide substitution on GPR30-mediated PI3K activation was observed for compounds **4−7**. Compounds **4** and **7** exhibited partial agonist properties on PI3K, acting as agonists when applied to cells in the absence of estrogen but also demonstrating the ability to inhibit the full activation of PI3K by estrogen. Compound **5** was a weaker agonist of PI3K than **3**, and compound **6** had no functional effect. Compounds **8** and **9** were able to block the estrogen-induced PI3K activation via GPR30 and thus appear to function as antagonists of GPR30 function in this context.

Because rapid signaling via GPR30 results in increased intracellular calcium levels,[5] we investigated whether compounds **3−9** had similar agonist and antagonist properties in a cell-based calcium assay using SKBr3 cells, which endogenously express only GPR30. In these cells, stimulation with GPR30 agonists, including estrogen and **1**, elicits a rapid increase in intracellular calcium levels that can be easily monitored using the cell-permeant fluorescent calcium indicator Indo-1. Consistent with the PI3K activation profiles, compounds **8** and **9** blocked estrogen-induced calcium mobilization and thus functioned as antagonists of estrogen-mediated GPR30 function. Additionally, compound **4** appears to weakly antagonize estrogen-mediated calcium mobilization. Compounds **3** and **5−7** can all be characterized as partial agonists in the context of this assay, as all compounds mobilize calcium when applied alone and all four compounds display some degree of inhibition of estrogen-mediated calcium mobilization. However, as in the PI3K assay, compound **3** is a potent agonist of calcium mobilization similar to **1**.

Some variability in compound profiles exists between the two GPR30 functional assays (i.e., compound **6** was inactive in the PI3K assay but a partial agonist of GPR30 in the calcium assay and compound **3** is a potent agonist in the PI3K assay and a partial, though still potent, agonist in the calcium assay). This is potentially due to the different cellular systems used in the assays and also may be related to assay sensitivity and the differing time courses of the assays. The PI3K assay employs ectopically expressed receptors in cells which may lack required cofactors for full compound activity; thus, some compounds may elicit weaker or no responses in this system than in a system in which cells with endogenous receptor are used, such as the calcium assay used to profile the compounds. Additionally, the PI3K assay is a phenotypic assay in which many fields of cells must be analyzed and an average response determined relative to control stimulated cells, whereas the calcium assay is a more quantitative assay in which smaller changes in signaling are more likely to be observed. Importantly, compounds **8** and **9** displayed consistent activity as antagonists of GPR30 function in both functional assays.

Table 2. In Vivo Biodistribution (% ID/g) of GPR30-Targeted Radioiodinated Tracer

| | 1 h PI | | 2 h PI | | 2 h PI (block)[a] | |
organ	8*	9*	8*	9*	8*	9*
heart	2.03 ± 0.35	5.23 ± 0.52	1.36 ± 0.09	3.52 ± 0.09	1.50 ± 0.36	3.72 ± 1.19
blood	3.18 ± 0.45	14.29 ± 1.25	3.14 ± 0.40	13.02 ± 2.42	2.23 ± 0.43	9.01 ± 0.56
lung	2.51 ± 0.14	7.97 ± 1.04	2.63 ± 0.51	7.32 ± 1.75	1.77 ± 1.19	5.21 ± 1.30
liver	6.31 ± 0.81	7.01 ± 1.46	5.88 ± 0.18	4.83 ± 0.42	6.74 ± 0.60	5.20 ± 1.94
spleen	2.65 ± 0.96	5.49 ± 0.31	2.08 ± 0.21	5.50 ± 1.35	2.22 ± 0.52	5.94 ± 1.30
large intestine	26.12 ± 5.53	8.04 ± 1.83	8.14 ± 0.87	5.40 ± 0.50	4.99 ± 0.85	9.11 ± 2.48
small intestine	9.56 ± 4.90	9.86 ± 0.86	3.83 ± 0.87	9.76 ± 2.04	2.86 ± 1.00	7.82 ± 4.19
stomach	4.51 ± 1.75	24.04 ± 7.39	5.42 ± 2.38	36.35 ± 4.24	3.84 ± 1.72	29.99 ± 3.34
kidney	6.76 ± 2.71	7.05 ± 0.42	1.90 ± 0.13	5.52 ± 0.52	3.60 ± 0.62	5.30 ± 1.76
adrenal[b]	2.15 ± 0.14	6.24 ± 1.04	1.70 ± 0.13	5.44 ± 0.40	0.99 ± 0.11	3.25 ± 0.52
bone	0.76 ± 0.03	1.86 ± 0.26	0.48 ± 0.09	2.72 ± 0.25	0.69 ± 0.14	2.03 ± 0.75
muscle	1.14 ± 0.56	1.36 ± 0.08	0.52 ± 0.05	1.30 ± 0.14	0.70 ± 0.07	1.42 ± 0.58
uterus[b]	1.42 ± 0.25	5.33 ± 0.64	2.83 ± 0.51	3.55 ± 0.33	0.67 ± 0.23	1.67 ± 0.10
mammary[b]	1.35 ± 0.26	5.01 ± 0.63	2.04 ± 0.10	3.33 ± 0.26	0.63 ± 0.15	2.23 ± 0.61
brain	0.14 ± 0.02	0.52 ± 0.27	0.10 ± 0.04	0.41 ± 0.10	0.08 ± 0.07	0.64 ± 0.15
urinary bladder	1.72 ± 0.86	7.03 ± 1.01	0.43 ± 0.10	4.00 ± 1.10	0.26 ± 0.07	5.60 ± 1.80
tumor[b]	0.99 ± 0.03	4.41 ± 0.25	1.08 ± 0.15	3.47 ± 0.17	0.56 ± 0.08	1.98 ± 0.50

[a] Receptor blocking studies performed by co-injecting 5 μg of **1** with the radiotracer. [b] Uptake values at 2 h PI are significantly different ($p < 0.05$) from the values at 2 h PI when the radiotracer was co-injected with 5 μg of **1** for blocking the receptor.

[125]**I Radiolabeling and GPR30 Binding.** The iodides **8** and **9** were selected for radiolabeling based on the results of the binding and functional assays combined with considerations of their chemical properties and synthetic accessibility of the tributylstannylated precursors. Although compound **3** exhibited a favorable GPR30-selective binding and functional profile, efforts to prepare the tributylstannyl precursor **12** were unsuccessful. The tributylstannyl precursor, *N*-{2-[4-(6-bromo-benzo[1,3]dioxol-5-yl)-3a,4,5,9b-tetrahydro-3*H*-cyclopenta[*c*]quinolin-8-yl]ethyl}-4-tributylstannylbenzamide for **7** was synthesized but not selected for ^{125}I labeling because of the poor solubility characteristics. Radioiodinated **8*** and **9*** were prepared using the iodogen method from tributylstannyl precursors **21** and **22**, respectively. A 1:1 stoichiometry of ^{125}I/:tributylstannyl precursor was used for radiolabeling and greatly simplified the purification process by avoiding the need to separate excess precursor. Typical radiochemical yields ranged from 40% to 55%. Over 99.9% unincorporated ^{125}I and unlabeled ligands were successfully separated from the radioiodinated **8*** and **9*** using solid phase extraction as determined by thin layer chromatography. The experimental log $P_{o/w}$ values of 7.0 ± 0.3 and 6.0 ± 0.2 for **8*** and **9*** determined by the shake-tube method were similar to the corresponding calculated values of 7.00 and 6.35 and followed the same relative ordering of lipophilicity **8** > **9**.

Competition binding studies were performed on adherent monolayers of GPR30-expressing human endometrial Hec50 cancer cells. The IC_{50} values of **6**, **7**, **8**, and **9** were 1.7, 16.2, 8.4, and 1.7 nM, respectively (Table 1). This binding assay was verified by evaluating the receptor binding affinity for the GPR30 agonist **1** ($IC_{50} \approx 7$ nM), which compares similarly to the value obtained using a competitive binding assay with a fluorescent estrogen ligand and recombinant GPR30 ($IC_{50} \approx 11$ nM),[13] and reported values for 17β-estradiol ($IC_{50} \approx 3-6$ nM).[5,6] The recently described GPR30 antagonist **2** exhibited slightly weaker binding ($IC_{50} \approx 20$ nM) relative to **1**.[26]

In Vivo Studies. In vivo biodistribution studies were performed on female ovariectomized athymic (NCr) nu/nu mice bearing GPR30-expressing human endometrial Hec50 tumors by intravenously injecting trace amounts of radioiodinated **8*** and **9***. Both the radiotracers **8*** and **9*** were rapidly metabolized and eliminated via the hepatobiliary system (gall bladder uptake of over 30% ID/g). Radiotracer **8*** was rapidly cleared from the intestines, kidney, and urinary bladder (Table 2).

However, increased uptake and retention was observed in the uterus, adrenal and mammary glands, and tumor, indicative of receptor-mediated uptake. Blocking studies also revealed GPR30-mediated uptake of **8*** in tumor, adrenal, and reproductive organs, sites of known or expected GPR30 expression. Radiotracer **9*** demonstrated a significantly different pharmacokinetic profile than radiotracer **8*** (Table 2). The blood uptake values of **9*** were nearly 3-fold that of **8*** at 1 h PI (14.3% ID/g vs 3.2% ID/g), indicative of high plasma-protein binding. However, blocking studies also revealed GPR30-mediated uptake of **9*** in tumor, adrenal, and reproductive organs. In spite of receptor-mediated uptake, the tumor was not visualized by a whole body 80 s/ projections SPECT/CT studies due to poor targeting characteristics of both the radiotracers (Supporting Information, S10). Quantitative SPECT/CT studies revealed further disparities between **8*** and **9***. The thyroid uptake of **9*** was almost 7 times greater than that of **8*** (4.1% ID vs 0.6% ID). Whereas the gall bladder (with bile content) uptake of **9*** was nearly 3 times lower than that of **8*** (1.8% ID vs 5.7% ID). For **8***, the organ with the largest uptake was intestine (over 70% ID), whereas for **9*** it was the stomach (over 15% ID). The imaging studies suggest that **8*** is less susceptible to in vivo dehalogenation compared to **9*** but was also more susceptible to metabolism because of increased gall bladder activity. The moderate increase in kidney uptake of compound **8*** upon coadministration of excess **1** could be due changes in metabolism or excretion kinetics in the presence of large doses of blocking agent. The high stomach uptake of **9*** could presumably be associated with the presence of free iodide, which would also correspond with the high thyroid levels observed. The blocking studies using the structurally related agonist **1** verified the critical involvement of GPR30-mediated uptake of the radiotracers; however, the corresponding displacement by **E2** was not characterized. This represents a limitation of the present study, since endogenous estrogens constitute the dominant competing ligands in

intact (not ovariectomized) animals and, although challenging to address experimentally, should be incorporated into the evaluation of next generation agents that exhibit improved targeting characteristics.

Conclusions

In this study, we developed a series of iodinated compounds that exhibit high affinity and selectivity toward GPR30 versus the classical estrogen receptors. The synthetic compounds were characterized using cell-based competitive binding and functional assays to identify binding affinity, specificity, and agonist or antagonist response associated with receptor-mediated signaling pathways. Two compounds incorporating either conjugated phenylurea or hydrazone linkages, respectively, were selected for radiolabeling with ^{125}I to provide **8*** and **9***. These compounds functioned as antagonists of GPR30-mediated calcium mobilization and were used for competitive ligand binding assays in cell culture. Comparative in vivo studies were used to evaluate the biodistribution, pharmacokinetics, and the potential for GPR30-targeted tumor imaging in an animal model. Although both radio-tracers **8*** and **9*** exhibited receptor-mediated uptake in tumor, adrenal, and reproductive organs, neither was effective for tumor imaging due to poor targeting characteristics, high background, and issues with plasma protein binding and rapid metabolism. The striking differences in the in vivo characteristics of **8*** and **9*** reflect the structural, physico-chemical, and metabolic differences associated with the iodinated appendages used. Dehalogenation, high plasma-protein binding, and uptake in the stomach were problematic for the *m*-iodophenylurea **9***. The iodopyridin-2-ylhydrazone **8*** was less susceptible to dehalogenation but exhibited increased metabolism and high uptake in the intestine. Both compound classes were significantly more lipophilic than either estradiol or the GPR30-selective probes **1** and **2**, which likely contributes toward the observed nontarget tissue uptake. The in vivo data from **8*** and **9*** provide valuable insight for the design of the next generation of GPR30-targeted radiotracers. The iodide **3** exhibited favorable characteristics including reduced lipophilicity and high selectivity as a GPR30 agonist; however, the inaccessibility of the tributylstannyl precursor through the synthetic routes investigated prevented further evaluation of the radioiodinated compound. It may be possible to incorporate the less sterically demanding trimethylstannyl group, which could serve as a precursor for ^{125}I labeling to yield this promising agent.[44] We have previously described ^{99m}Tc-labeled 17β-estradiol derivatives that incorporate pyridin-2-yl-hydrazine chelates for SPECT imaging applications.[45,46] These studies suggest that incorporating this ^{99m}Tc-imaging modality into the tetrahydrocyclopenta[c]-quinoline scaffold could result in GPR30-selective agents with decreased lipophilicity, increased chemical and metabolic stability, reduced plasma-protein binding, and overall improvements in targeting characteristics for in vivo imaging applications.

Experimental Section

General Methods. Reagents and solvents were obtained from commercial sources and used without further purification. Chromatographic separations were performed using medium pressure flash chromatography and ethyl acetate/hexanes or methanol/dichloromethane as eluent. Reverse phase chromatography employed C-18 columns and water-acetonitrile or water−methanol mobile phase. NMR spectra were acquired at ambient temperatures (18 ± 2 °C) unless otherwise noted. Reactions were monitored by thin-layer chromatography on silica gel (60 Å pore size, 5−17 μm) polyester backed sheets that were visualized under a UV lamp, iodine vapor, phosphomolybdic acid, or anisaldehyde. The ^{1}H NMR spectra in CDCl$_3$ were referenced to TMS unless otherwise noted. The ^{13}C {^{1}H} NMR spectra were recorded at 75 or 100 MHz and referenced relative to the ^{13}C {^{1}H} peaks of the solvent. Spectra are reported as follows: shift (ppm), multiplicity, coupling constants (Hz), and number of protons. Melting points are uncorrected. The purity of all compounds used in biological studies was determined to be > 95% by analytical HPLC equipped with photodiode array (PDA) and ESI-MS detection. The compounds (1 mg/mL CH$_3$CN, 20 μL) were injected into a Waters Symmetry C$_{18}$ 5 μm, 3.0 mm × 150 mm column and eluted as specified. Reported binding and functional characterization values are based on a minimum of three measurements.

General Procedure for Sc(OTf)$_3$ Mediated Cyclization. A catalytic amount of Sc(OTf)$_3$ (10 mol %) in anhydrous acetonitrile (0.5 mL) was added to a mixture of 6-bromopiperonal (1 equiv), aniline derivative (1 equiv), and cyclopentadiene (5 equiv) in acetonitrile (4 mL). The reaction mixture was stirred at ambient temperature (~23 °C) for 2−5 h with monitoring of the product formation by thin layer chromatography using ethyl acetate/hexanes as eluent. The volatiles were removed in vacuo. The crude product was purified as specified.

1-[4-(6-Iodobenzo[1,3]dioxol-5-yl)-3a,4,5,9b-tetrahydro-3*H*-cyclopenta[*c*]quinolin-8-yl]ethanone (3). According to the general procedure, 6-iodopiperonal (0.055 g, 0.2 mmol), *p*-aminoacetophenone (0.027 g, 0.2 mmol), cyclopentadiene (0.066 g, 1.0 mmol), and Sc(OTf)$_3$ (0.010 g, 0.5 mmol) were combined with a reaction time of 2 h. The volatiles were removed in vacuo. The residue was purified by preparative silica gel column chromatography using ethyl acetate/hexanes (10:90) to provide **3** (0.085 g, 92%) as a colorless solid. Mp 106−109 °C; IR (KBr, cm^{-1}) 3320, 2880, 1665, 1575, 1242; ^{1}H NMR (400 MHz, CDCl$_3$) δ 7.71 (d, *J* = 1.9 Hz, 1H), 7.62 (dd, *J* = 8.4, 1.9 Hz, 1H), 7.28 (s, 1H), 7.07(s, 1H), 6.61 (d, *J* = 8.4 Hz, 1H), 6.01 (d, *J* = 1.1 Hz, 1H), 5.99 (d, *J* = 1.1 Hz, 1H), 5.96−5.94 (m, 1H), 5.68−5.66 (m, 1H), 4.82 (d, *J* = 3.1 Hz, 1H), 4.14 (d, *J* = 8.8 Hz, 1H), 4.06 (bs, 1H), 3.19−3.13 (m, 1H), 2.56−2.44 (m, 4H), 1.83−1.79 (m, 1H); ^{13}C NMR (75 MHz, CDCl$_3$) δ 196.5, 149.8, 148.6, 147.8, 136.3, 133.7, 130.4, 130.0, 128.6, 127.6, 125.1, 118.9, 115.2, 107.9, 101.7, 60.8, 45.3, 42.2, 31.2, 26.0. HPLC−MS: Elution with 60−90% CH$_3$CN (gradient 1.5% min^{-1}) in H$_2$O exhibited a single peak at 12.38 min. ESI-MS *m/z* [ES+] calcd for C$_{21}$H$_{18}$INO$_3$ [M + H]$^+$ 460.03; found 460.09.

1-(4-(6-Bromobenzo[d][1,3]dioxol-5-yl)-6-iodo-3a,4,5,9b-tetrahydro-3*H*-cyclopenta[*c*]quinolin-8-yl)ethanone (4). According to the general procedure 6-bromopiperonal (0.115 g, 0.5 mmol), 1-(4-amino-3-iodophenyl)ethanone (0.140 g, 0.53 mmol), cyclopentadiene (0.165 g, 2.5 mmol), and Sc(OTf)$_3$ (0.0246 g, 0.5 mmol) were combined with a reaction time of 3 h. The volatiles were removed in vacuo. The residue was purified by preparative silica gel column chromatography using ethyl acetate/hexanes (08:92) to provide **4** (0.151 g, 56%) as a white solid. Mp 110−114 °C; IR (KBr, cm^{-1}) 3447, 2920, 1670, 1588, 1476, 1242; ^{1}H NMR (300 MHz, CDCl$_3$) δ 8.11 (d, *J* = 2.0 Hz, 1H), 7.65 (d, *J* = 2.0 Hz, 1H), 7.14 (s, 1H), 7.06 (s, 1H), 6.03 (d, *J* = 1.3 Hz, 1H), 6.02 (d, *J* = 1.3 Hz, 1H), 5.92−5.88 (m, 1H), 5.68−5.66 (m, 1H), 4.99 (d, *J* = 3.5 Hz, 1H), 4.53 (bs, 1 H), 4.14 (d, *J* = 8.2 Hz, 1H), 3.25−3.19(m, 1H), 2.52−2.42 (m, 4H), 1.87−1.77 (m, 1H); ^{13}C NMR (75 MHz, CDCl$_3$) δ 195.1, 148.9, 147.7, 147.6, 137.3, 133.4, 132.9, 130.7, 129.6, 129.6, 125.6, 113.0, 107.4, 101.8, 85.4, 77.2, 56.6, 45.9, 42.3, 31.4, 25.9. HPLC−MS: Elution with 60−90% CH$_3$CN in H$_2$O (gradient 1.5% min^{-1}) exhibited a single peak at 17.40 min. HRMS: calcd for C$_{21}$H$_{17}$BrINO$_3$ [M + H]$^+$ 537.9515; found 537.9525.

4-(6-Bromobenzo[1,3]dioxol-5-yl)-7-iodo-3a,4,5,9b-tetrahydro-3*H*-cyclopenta[*c*]quinoline (5). According to the general procedure

6-bromopiperonal (0.229 g, 1 mmol), *m*-iodoaniline (0.219 g, 1 mmol), cyclopentadiene (0.330 g, 5 mmol), and Sc(OTf)$_3$ (0.0492 g, 0.1 mmol) were combined with a reaction time of 2 h. The volatiles were removed in vacuo. The residue was purified by preparative silica gel column chromatography using ethyl acetate/hexanes (10:90) to provide **5** (0.354 g, 72%) as a white solid. Mp 195−198 °C; IR (KBr, cm^{-1}) 3432, 2881, 1573, 1496, 1217; ^{1}H NMR (300 MHz, CDCl$_3$) δ 7.01 (s, 1H), 7.05 (dd, J = 8.0, 2.0 Hz, 1H), 7.03 (s, 1H), 6.97 (d, J = 2.0 Hz, 1H), 6.77 (d, J = 8.0 Hz, 1H), 6.00 (d, J = 1.5 Hz, 1H), 5.98 (d, J = 1.5 Hz, 1H), 5.83−5.79 (m, 1H), 5.69−5.64 (m, 1H), 4.87 (d, J = 3.3 Hz, 1H), 4.03 (d, J = 9 Hz, 1H), 3.55 (bs, 1H), 3.21−3.09 (m, 1H), 2.58−2.49 (m, 1H), 1.84−1.75 (m, 1H); ^{13}C NMR (75 MHz, CDCl$_3$) δ 147.5, 147.3, 146.8, 133.9, 133.4, 130.6, 130.5, 128.1, 125.7, 124.4, 113.0, 112.9, 107.8, 101.7, 101.7, 90.9, 56.3, 45.6, 40.9, 31.3. HPLC−MS: Elution with 73:27 CH$_3$CN/H$_2$O containing 0.01% formic acid exhibited a single peak at t_R = 22.38 min. HRMS: calcd for C$_{19}$H$_{15}$BrINO$_2$ [M + H]$^+$ 495.9409; found 495.9412.

4-(6-Bromobenzo[1,3]dioxol-5-yl)-8-iodo-3a,4,5,9b-tetrahydro-3H-cyclopenta[c]quinoline (6). According to the general procedure, 6-bromopiperonal (0.460 g, 2 mmol), *p*-iodoaniline (0.438 g, 2 mmol), cyclopentadiene (0.66 g, 10 mmol), and Sc(OTf)$_3$ (0.098 g, 0.2 mmol, 10 mol %) were combined with a reaction time of 2 h. The product **6** (0.890 g, 90%) was isolated by filtration as a white solid. Mp 175−178 °C; IR (KBr, cm^{-1}) 3435, 2887, 1588, 1481, 1239; ^{1}H NMR (300 MHz, CDCl$_3$) δ 7.33 (d, J = 2.0 Hz, 1H), 7.23 (dd, J = 8.4, 2.0 Hz, 1H), 7.11 (s, 1H), 7.02 (s, 1H), 6.38 (d, J = 8.4 Hz, 1H), 5.99 (d, J = 1.2 Hz, 1H), 5.98 (d, J = 1.2 Hz, 1H), 5.84−5.80 (m, 1H), 5.68−5.66 (m, 1H), 4.85 (d, J = 3.3 Hz, 1H), 4.05 (d, J = 9.0 Hz, 1H), 3.5 (bs, 1H), 3.20−3.09 (m, 1H), 2.59−2.48 (m, 1H), 1.84−1.74 (m, 1H); ^{13}C NMR (75 MHz, CDCl$_3$) δ 147.5, 147.3, 145.0, 137.5, 134.3, 134.0, 133.4, 130.7, 128.8, 118.5, 113.0, 112.9, 107.9, 101.7, 80.5, 56.4, 45.7, 41.9, 31.3. HPLC−MS: Elution with 73:27 CH$_3$CN/H$_2$O containing 0.01% formic acid exhibited a single peak at t_R = 22.10 min. HRMS: calcd for C$_{19}$H$_{15}$BrINO$_2$ [M + H]$^+$ 495.9409; found 495.9407.

N-{2-[4-(6-Bromobenzo[1,3]dioxol-5-yl)-3a,4,5,9b-tetrahydro-3H-cyclopenta[c]quinolin-8-yl]ethyl}-4-iodobenzamide (7). The amine **10** (0.082 g, 0.2 mmol) and 4-iodobenzoic acid (0.049 g, 0.2 mmol) were combined in dry DMF (1 mL). Diisopropylethylamine (0.025 g, 0.2 mmol) was added, followed by the addition of benzotriazol-1-yl-oxytripyrrolidinophosphonium hexafluorophosphate (0.103 g, 0.2 mmol) and allowed to stir at ambient temperature for 20 h. The precipitate formed was filtered and washed with water and dried in vacuo to provide **10** (0.100 g, 78%) as a white solid. Mp 217−220 °C; IR (KBr, cm^{-1}) 3338, 1631, 1481, 1244, 1038; ^{1}H NMR (300 MHz, DMSO-d_6) δ 8.58 (t, J = 5.4 Hz, 1H), 7.85 (d, J = 8.4 Hz, 2H), 7.61 (d, J = 8.4 Hz, 2H), 7.24 (s, 1H), 7.14 (s, 1H), 6.84 (m, 1H), 6.77 (dd, J = 8.1, 1.7 Hz, 1H), 6.63 (d, J = 8.1 Hz, 1H), 6.09 (s, 1H), 6.07 (s, 1H), 5.82−5.77 (m, 1H), 5.58−5.55 (m, 1H), 5.47 (bs, 1H), 4.62 (d, J = 3.0 Hz, 1H), 3.96 (d, J = 8.9 Hz, 1H), 3.34−3.38 (m, 2H), 3.04−2.96 (m, 1H), 2.67 (t, J = 7.3 Hz, 2H), 2.45−2.38 (m, 1H), 1.68−1.60 (m, 1H); ^{13}C NMR (75 MHz, DMSO-d_6) δ 165.3, 147.0, 146.9, 144.3, 137.5, 137.0, 134.3, 134.0, 131.0, 129.4, 129.1, 128.7, 126.1, 124.8, 116.1, 112.3, 112.1, 108.5, 101.8, 98.5, 56.0, 45.54, 41.8, 41.3, 34.3, 31.1. HPLC−MS: Elution with 60−90% CH$_3$CN in H$_2$O (gradient 1.5% min^{-1}) exhibited a single peak at 15.98 min. HRMS: calcd for C$_{28}$H$_{24}$BrIN$_2$O$_3$ [M + H]$^+$ 664.9913; found 664.9916.

1-{2-[4-(6-Bromobenzo[1,3]dioxol-5-yl)-3a,4,5,9b-tetrahydro-3H-cyclopenta[c]quinolin-8-yl]ethyl}-3-(3-iodophenyl)urea (8). A solution of 3-iodophenyl isocyanate (0.10 g, 0.4 mmol) in dry DMF (1 mL) was added to the amine **10** (0.082 g, 0.2 mmol) and Et$_3$N (0.02 g, 0.2 mmol) in dry DMF (1 mL) in an ice bath and allowed to stir overnight at ambient temperature. The reaction mixture washed with water (15 mL), and the product was extracted with methylene chloride (30 mL). The organic layer was dried over anhydrous sodium sulfate and evaporated under reduced pressure. The residue was purified by silica gel column

chromatography using ethyl acetate/hexanes (25:75) to provide **8** (0.09 g, 67%) as a white solid. Mp 210−213 °C; IR (KBr, cm^{-1}) 3290, 1636, 1580, 1474; ^{1}H NMR (300 MHz, DMSO-d_6) δ 8.60 (s, 1H), 7.98−7.97 (m, 1H), 7.25−7.20 (m, 3H), 7.14 (s, 1H), 7.01−6.96 (m, 1H), 6.85 (s, 1H), 6.76 (dd, J = 8.2, 1.76 Hz, 1H), 6.65 (d J = 8.1, 1H), 6.11−6.05 (m, 3H), 5.87−5.83 (m, 1H), 5.58−5.53 (m, 1H), 5.45 (bs, 1H), 4.63 (d, J = 2.8 Hz, 1H), 3.97 (d, J = 8.8 Hz, 1H), 3.28−3.22 (m, 2H), 3.05−2.95 (m, 1H), 2.62−2.54 (m, 2H), 2.45−2.40 (m, 1H), 1.69−1.60 (m, 1H); ^{13}C NMR (75 MHz, DMSO-d_6) δ 154.7, 147.0, 146.9, 144.3, 142.0, 134.6, 134.3, 130.58, 129.4, 129.3, 128.6, 126.1, 125.6, 124.9, 116.7, 116.1, 112.3, 112.1, 108.5, 101.8, 94.7, 56.0, 45.5, 41.8, 40.8, 40.3, 35.0, 31.1. HPLC−MS: Elution with 63−93% CH$_3$CN in H$_2$O containing 0.01% formic acid (gradient 1% min^{-1}) exhibited a two peaks at t_R = 26.40 min (*exo*) and 27.88 min (*endo*). HRMS: calcd for C$_{28}$H$_{25}$BrI-N$_3$O$_3$ [M + H]$^+$ 658.0202; found 658.0193.

N-{1-[4-(6-Bromobenzo[1,3]dioxol-5-yl)-3a,4,5,9b-tetrahydro-3H-cyclopenta[c]quinolin-8-yl]ethylidene}-N′-(5-iodopyridin-2-yl)-hydrazine (9). The (5-iodopyridin-2-yl)hydrazine (0.047 g, 0.2 mmol) was heated with **1** (0.082 g, 0.2 mmol) at 170−180 °C for 5 min in vacuo (2 mmHg). The crude hydrazone was purified by reverse phase column chromatography using acetonitrile/water (75:25) to provide **9** (0.101 g, 85%) as a pale-yellow solid. Mp 128−131 °C. IR (KBr, cm^{-1}) 3351, 2919, 1611, 1578, 1493; ^{1}H NMR (300 MHz, CDCl$_3$) δ 8.26 (d, J = 1.8 Hz, 1H), 7.98 (s, 1H), 7.79 (dd, J = 8.8, 2.0 Hz, 1H), 7.43−7.40 (m, 2H), 7.24−7.18 (m, 1H), 7.13 (s, 1H), 7.02 (s, 1H), 6.61 (d, J = 8.2 Hz, 1H), 5.98 (d, J = 1.3 Hz, 1H), 5.97 (d, J = 1.3 Hz, 1H) 5.93−5.899 (m, 1H), 5.68−5.63 (m, 1H), 4.89 (d, J = 3.1 Hz, 1H), 4.13 (d, J = 8.8 Hz, 1H), 3.69 (s, 1H), 3.23−3.16 (m, 1H), 2.60−2.51 (m, 1H), 2.16 (s, 3 H), 1.84−1.76 (m, 1H); ^{13}C NMR (75 MHz, CDCl$_3$) δ 156.2, 153.0, 147.4, 147.2, 146.0, 145.5, 144.5, 134.1, 133.9, 130.3, 129.7, 126.5, 125.6, 124.1, 115.9, 113.0, 112.8, 109.8, 107.9, 101.7, 79.2, 56.5, 45.9, 42.1, 31.3, 12.3. HPLC-MS: Elution with 73:27 CH$_3$CN/H$_2$O containing 0.01% formic acid exhibited two peaks at t_R = 17.18 min (*exo*) and 22.33 min (*endo*). HRMS: calcd for C$_{26}$H$_{22}$BrIN$_4$O$_2$ [M + H]$^+$ 629.0049; found 628.9939.

1-[2-(4-Aminophenyl)ethyl]-3-(3-iodophenyl)urea (19). A solution of 3-iodophenyl isocyanate (0.490 g, 2.0 mmol) in dry dichloromethane (10 mL) was added to 4-aminophenethylamine (0.272 g, 2.0 mmol) in an ice bath and subsequently allowed to stir for 2 h at ambient temperature. The white solid precipitate was separated by centrifugation and dried in vacuo to provide **19** (0.703 g, 92%) as a colorless solid. Mp 161−163 °C; IR (KBr, cm^{-1}) 3312, 1628, 1577, 1516, 1472; ^{1}H NMR (300 MHz, DMSO-d_6) δ 8.60 (s, 1H), 7.96 (t, J = 1.76 Hz, 1H), 7.24−7.18 (m, 2H), 6.98 (t, J = 8.0 Hz, 1H), 6.86 (d, J = 8.3 Hz, 2H), 6.50 (d, J = 8.3 Hz, 2H), 6.09−6.05 (m, 1H), 4.84 (s, 2H), 3.25−3.18 (m, 2H), 2,54 (t, J = 7.19 Hz, 2H); ^{13}C NMR (75 MHz, DMSO-d_6) δ 154.7, 147.7, 142.0, 130.6, 129.3, 128.9, 126.1, 125.5, 116.7, 114.0, 94.7.

1-[2-(4-Aminophenyl)ethyl]-3-(3-tributylstannanylphenyl)urea (20). A mixture of 1-[2-(4-aminophenyl)ethyl]-3-(3-iodophenyl)urea (0.381 g, 1 mmol), bistributyltin (1.16 g, 2 mmol), and tetrakis(triphenylphosphine)palladium (0.115 g, 0.10 mmol) was refluxed in dry dioxane at 100 °C for 3 h under argon. The volatiles were removed in vacuo. The residue was purified by preparative silica gel column chromatography using ethyl acetate/hexanes (40:60) to provide **20** (0.331 g, 61%) as a colorless liquid. IR (KBr, cm^{-1}) 3410, 2920, 2912, 1632, 1238; ^{1}H NMR (300 MHz, CDCl$_3$) δ 7.30 (d, J = 1.4 Hz, 1H), 7.23−7.20 (m, 2H), 7.14−7.12 (m, 1H), 6.92 (d, J = 8.3 Hz, 2H), 6.80 (s, 1H), 6.56 (d, J = 8.3 Hz, 2H), 5.13 (t, J = 5.7 Hz, 1H), 3.48 (bs, 2H), 3.37 (q, J = 6.0 Hz, 2H), 2.65 (t, J = 7.0 Hz, 2H), 1.56−1.46 (m, 6H), 1.36−1.24 (m, 6H), 1.06−1.00 (m, 6H), 0.86 (t, J = 7.4 Hz, 9H); ^{13}C NMR (75 MHz, CDCl$_3$) δ 156.0, 144.6, 143.1, 138.1, 131.6, 129.5, 128.8, 128.5, 128.4, 120.7, 115.3, 41.6, 35.3, 29.1, 27.3, 13.6, 9.5. HPLC−MS: Elution with 60−90% CH$_3$CN in H$_2$O (gradient 1% min^{-1}) exhibited a single peak at t_R = 24.60 min.

ESI-MS m/z (ES+) calcd for $C_{27}H_{43}N_3OSn$ [M + Na]$^+$ 568.23; found 568.09.

(1-{2-[4-(6-Bromobenzo[1,3]dioxol-5-yl)-3a,4,5,9b-tetrahydro-3H-cyclopenta[c]quinolin-8-yl]ethyl}-3-(3-tributylstannylphenyl)-urea) (21). According to the general procedure, 6-bromopiperonal (0.034 g, 0.147 mmol), **20** (0.080 g, 0.147 mmol), cyclopentadiene (0.048 g, 0.735 mmol), and Sc(OTf)$_3$ (0.007 g, 0.014 mmol) were combined with a reaction time of 8 h. The volatiles were removed in vacuo. The residue was purified by preparative silica gel column chromatography using ethyl acetate/hexanes (35:65) to provide **21** (0.090 g, 75%) as a white solid. Mp 125−127 °C; IR (KBr, cm^{-1}): 3336, 2955, 2924, 1635, 1564, 1241; ^{1}H NMR (300 MHz, CDCl$_3$) δ 7.25−7.16 (m, 6H), 7.02 (s, 1H), 6.68(s, 1H), 6.80 (dd, $J = 7.7, 1.4$ Hz, 1H), 6.55 (d, $J = 8.0$ Hz, 1H), 6.22 (bs, 1H), 5.99 (d, $J = 1.3$ Hz, 1H), 5.98 (d, $J = 1.3$ Hz, 1H), 5.82−5.79 (m, 1H), 5.66−5.60 (m, 1H), 4.84 (d, $J = 2.8$ Hz, 1H), 4.78 (bs, 1H), 4.05 (d, $J = 8.2$ Hz, 1H), 3.47 (q, $J = 5.8$ Hz, 2H), 3.21−3.10 (m, 1H), 2.71 (t, $J = 6.9$ Hz, 2H), 2.60−2.51 (m, 1H), 1.83−1.74 (m, 1H), 1.57−1.47 (m, 6H), 1.37−1.25 (m, 6H), 1.06−1.01 (m, 6H), 0.87 (t, $J = 7.4$ Hz, 9H); ^{13}C NMR (75 MHz, CDCl$_3$) δ 155.9, 147.4, 147.2, 143.6, 143.3, 138.0, 134.4, 133.9, 131.9, 130.2, 129.2, 128.87, 128.85, 128.5, 126.6, 126.3, 121.0, 116.3, 113.0, 112.8, 108.0, 101.7, 56.7, 45.9, 42.0, 41.7, 35.4, 31.2, 29.0, 27.3, 13.6, 9.5. HPLC−MS: Elution with 93:7 CH$_3$CN/H$_2$O containing 0.01% formic acid exhibited a single peak at t_R = 22.67 min. ESI-MS m/z [ES+] calcd for $C_{40}H_{52}BrN_3O_3Sn$ [M + H]$^+$ 822.22; found 822.20.

N-{1-[4-(6-Bromobenzo[1,3]dioxol-5-yl)-3a,4,5,9b-tetrahydro-3H-cyclopenta[c]quinolin-8-yl]ethylidene}-N'-(5-tributylstannanylpyridin-2-yl)hydrazine (22). A mixture of 2-chloro-5-tributylstannylpyridine (0.401 g, 1 mmol) and hydrazine hydrate (3 mL) was heated at 120 °C in pyridine (5 mL) for 24 h. The volatiles were removed by rotary evaporation. Sodium hydroxide (1 N, 25 mL) was added to the residue, and the product was extracted with dichloromethane (3 × 15 mL) and dried over anhydrous Na$_2$SO$_4$. The volatiles were removed in vacuo to provide (5-tributylstannanylpyridin-2-yl)-hydrazine. The hydrazine was heated with **1** (0.144 g, 0.35 mmol) at 170−180 °C for 5 min in vacuo (2 mmHg). The crude hydrazone was purified by reverse phase column chromatography using methanol/water (90:10) to provide **22** (0.180 g, 65%) as a pale-yellow solid. Mp 114−116 °C; IR (KBr, cm^{-1}) 3351, 2919, 1611, 1578, 1493; ^{1}H NMR (300 MHz, CDCl$_3$) δ 8.09−8.08 (m, 1H), 7.94 (bs, 1H), 7.65 (dd, $J = 8.2, 1.6$ Hz, 1H), 7.48 (d, $J = 1.6$ Hz, 1H), 7.44 (dd, $J = 8.3, 2.0$ Hz, 1H), 7.37 (dd, $J = 8.2, 1.0$ Hz, 1H), 7.16 (s, 1H), 7.03(s, 1H), 6.62 (d, $J = 8.3$ Hz, 1H), 5.99 (d, $J = 1.4$ Hz, 1H), 5.97 (d, $J = 1.4$ Hz, 1H), 5.94−5.91 (m, 1H), 5.70−5.64 (m, 1H), 4.90 (d, $J = 3.0$ Hz, 1H), 4.15 (d, $J = 8.6$ Hz, 1H), 3.67 (bs, 1H), 3.25−3.15 (m, 1H), 2.62−2.53 (m, 1H), 2.22 (s, 3H), 1.85 (m, 1H), 1.59−1.49 (m, 6H), 1.41−1.25 (m, 6H), 1.08−1.03 (m, 6H), 0.89 (t, $J = 7.2$ Hz, 9H); ^{13}C NMR (75 MHz, CDCl$_3$) δ 157.1, 153.7, 147.5, 147.2, 145.8, 145.7, 143.3, 134.2, 133.9, 130.3, 130.1, 126.4, 125.7, 125.4, 124.1, 115.8, 113.0, 112.8, 108.0, 107.9, 101.7, 56.6, 45.9, 42.1, 31.3, 29.0, 27.3, 13.6, 12.2, 9.5. HPLC−MS: Elution with 73:27 CH$_3$CN/H$_2$O containing 0.01% formic acid exhibited two peaks at t_R = 8.40 min (*exo*) and 11.08 min (*endo*). ESI-MS m/z [ES+] calcd for $C_{38}H_{49}BrN_4O_2Sn$ [M + H]$^+$ 793.21; found 793.23.

Radioiodination. The ^{125}I-labeled ligands **8*** and **9*** were prepared by oxidative radioiododestannylation of the corresponding tributylstannyl derivatives **21** and **22** using iodogen-coated reaction tubes (Thermo Fisher Scientific, Rockford, IL). The tributylstannyl precursor was dissolved in ethanol (5 μL) and allowed to stand at room temperature for 30 min with occasional gentle stirring. A 100 μL solution of 10 mM Tris (pH 7) was added to an iodogen-coated tube, followed by addition of sodium ^{125}I (~5 mCi, catalog no. NEZ033L005MC, Perkin-Elmer, Waltham, MA), followed by incubation at room temperature for 2−5 min. The tributylstannyl precursor (1 equiv in 5 μL) was added to the iodogen tube and incubated for 5 min. The reaction mixture was transferred to a new iodogen-coated tube and allowed to stand for an additional 1 h with occasional gentle stirring. The product was purified by solid phase extraction

using a reverse phase C18 Sep-pak column (Waters, Milford, MA). Unreacted ^{125}I and unlabeled ligand were eluted in distilled water (weak solvent), and ethanol was used to extract radioiodinated **8*** and **9***. To assess the iodination efficiency, thin-layer chromatography (TLC) was performed using silica gel strips (Gelman Sciences, Inc., Ann Arbor, MI). Ethanol and 0.9% (w/v) sodium chloride solutions were used as organic and aqueous mobile phases, respectively. The developed strips were scanned using a thin-layer-chromatography-imaging scanner (AR-2000, BioScan, Inc., Washington, DC). Ethanol was evaporated using nitrogen gas to obtain concentrated solutions of radioiodinated **8*** and **9***. The log $P_{o/w}$ values were experimentally determined using the shake-tube method as previously described.[45] For biological experiments, the concentrated ethanol solution was reconstituted in aqueous solutions containing 0.1% albumin, 0.1% Tween-20, and 10% ethanol.

Intracellular Calcium Mobilization. SKBr3 cells (1×10^7/mL) were incubated in HBSS containing 3 μM Indo1 a.m. (Invitrogen) and 0.05% pluronic acid F-127 for 1 h at room temperature. Cells were then washed twice with HBSS, incubated at room temperature for 20 min, washed again with HBSS, resuspended in HBSS at a density of 10^8cells/mL, and kept on ice until assay, performed at a density of 2×10^6 cells/mL. Ca^{2+} mobilization was determined ratiometrically using λ_{ex} of 340 nm and λ_{em} of 400/490 nm at 37 °C in a spectrofluorometer (QM-2000-2, Photon Technology International) equipped with a magnetic stirrer. The relative 490 nm/400 nm ratio was plotted as a function of time. All experiments were performed a minimum of three times.

PI3K Activation. The PIP3 binding domain of Akt fused to mRFP1 (PH-RFP) was used to localize cellular PIP3. COS7 cells (cotransfected with GPR30-GFP or ERα-GFP and PH-RFP) or SKBr3 (transfected with PH-RFP) cells were plated on coverslips, and serum was starved for 24 h followed by stimulation with ligands as indicated. The cells were fixed with 2% PFA in PBS, washed, mounted in Vectashield containing DAPI (Vector Labs), and analyzed by confocal microscopy using a Zeiss LSM510 confocal fluorescent microscope. All experiments were performed a minimum of three times.

Ligand Binding Assays. Binding assays for ERα and ERβ were performed as previously described.[5] Briefly, COS7 cells were transiently transfected with either ERα-GFP or ERβ-GFP. Following serum starvation for 24 h, cells (~5 × 10^4) were incubated with compounds **3**−**9** for 10 min in a final volume of 10 μL prior to addition of 10 μL of 20 nM E2-Alexa633 in saponin-based permeabilization buffer. Following 5 min at room temperature, cells were washed once with 1 mL of PBS/2%BSA, resuspended in 200 μL, and analyzed on a FACS Calibur flow cytometer (BD Biosciences).

For GPR30 binding, 1-{2-[4-(6-bromobenzo[1,3]dioxol-5-yl)-3a,4,5,9b-tetrahydro-3H-cyclopenta[c]quinolin-8-yl]ethyl}-3-(3-iodo(125)-phenyl)urea (**8***), was used. Briefly, Hec50 cells were cultured in phenol red free DMEM/F-12 containing 10% charcoal-stripped FBS, plated in 24-well tissue culture plates, and grown to 80% confluence. Wells were rinsed with PBS, and cells were incubated with competitor (**6**, **7**, **8**, **9**) for 30 min prior to addition of approximately 0.5−1 μCi of radioligand. Wells were incubated at 37 °C for 1 h and rinsed with PBS, and radioactivity was collected by ethanol extraction and counted in a Wallac Wizard 1480 γ counter (Perkin-Elmer, Gaithersburg, MD). All binding experiments were performed a minimum of three times.

Cell Culture. ERα/β-negative and GPR30-negative COS7 cells and ERα/β-negative and GPR30-expressing human endometrial carcinoma Hec50 cells were cultured in DMEM medium, fetal bovine serum (10%), 100 units/mL penicillin, and 100 μg/mL streptomycin. ERα/β-negative and GPR30-expressing SKBr3 cells were cultured in RPMI-1640 medium, fetal bovine serum (10%), 100 units/mL penicillin, and 100 μg/mL streptomycin. Cells were grown as a monolayer at 37 °C in a humidified atmosphere of 5% CO$_2$ and 95% air.

Animal Studies. All animal experiments were performed in accordance with the NIH Guide for the Care and Use of Laboratory Animals and were approved by the UNM Institutional Animal Care and Use Committee. A human endometrial carcinoma xenograft tumor model was developed by injecting 4 million Hec50 cells subcutaneously in 8-week-old female ovariectomized athymic (NCr) nu/nu mice (NCI-Frederick, Frederick, MD). After 4–6 weeks, tumors ranging from 0.7 to 0.9 cm in diameter were observed. Once the tumors were formed, biodistribution and SPECT/CT studies were performed. Hec50 tumor-bearing mice were injected intravenously (tail vein) with individual radioiodinated **8*** and **9***. To determine GPR30 receptor specificity, in a different set of experiments 5 μg of **1** was co-injected with the radiotracer. At the desired time points, animals were sacrificed by CO_2 euthanasia and organs were carefully removed and isolated to determine the biodistribution characteristics of the radiotracer. The organ samples were weighed, and the corresponding radioactivity was measured using an automated γ counter after verifying the counting efficiency with standards. The percent injected dose per gram of tissue (% ID/g) was calculated by comparison with standards representing the injected dose per animal.

NanoSPECT/CT imaging studies were performed using a multipinhole NanoSPECT/CT small animal imager (Bioscan Inc., Washington, DC). Whole body imaging studies were carried out using 1.5–1.7% isoflurane on a temperature controlled bed after injecting 2.5 MBq of radioiodinated derivatives in tumor-bearing mice.

Statistical Analysis. All numerical data were expressed as the mean of the values $\pm$ the standard error of mean (SEM). Graphpad Prism, version 4 (San Diego, CA), was used for statistical analysis, and a *P* value less than 0.05 was considered statistically significant.

Supporting Information Available: Additional synthetic procedures and characterization data; HPLC–MS data for **8, 9, 21, 22**; and SPECT/CT images of **8*** and **9***. This material is available free of charge via the Internet at http://pubs.acs.org.

References

(1) Edwards, D. P. Regulation of signal transduction pathways by estrogen and progesterone. *Annu. Rev. Physiol.* **2005**, *67*, 335–376.

(2) Lange, C. A.; Gioeli, D.; Hammes, S. R.; Marker, P. C. Integration of rapid signaling events with steroid hormone receptor action in breast and prostate cancer. *Annu. Rev. Physiol.* **2007**, *69*, 171–199.

(3) http://www.iuphar-db.org/GPCR/ReceptorDisplayForward?receptorID = 3055.

(4) Filardo, E. J.; Quinn, J. A.; Bland, K. I; Frackelton, A. R., Jr. Estrogen-induced activation of Erk-1 and Erk-2 requires the G protein-coupled receptor homolog, GPR30, and occurs via trans-activation of the epidermal growth factor receptor through release of HB-EGF. *Mol. Endocrinol.* **2000**, *14*, 1649–1660.

(5) Revankar, C. M.; Cimino, D. F.; Sklar, L. A.; Arterburn, J. B.; Prossnitz, E. R. A transmembrane intracellular estrogen receptor mediates rapid cell signaling. *Science* **2005**, *307*, 1625–1630.

(6) Thomas, P.; Pang, Y.; Filardo, E. J.; Dong, J. Identity of an estrogen membrane receptor coupled to a G-protein in human breast cancer cells. *Endocrinology* **2005**, *146*, 624–632.

(7) Prossnitz, E. R.; Arterburn, J. B.; Smith, O. H.; Oprea, T. I.; Sklar, L. A.; Hathaway, H. J. Estrogen signaling through the transmembrane G protein-coupled receptor GPR30. *Annu. Rev. Physiol.* **2008**, *70*, 165–190.

(8) Prossnitz, E. R.; Sklar, L. A.; Oprea, T. I.; Arterburn, J. B. GPR30: a novel therapeutic target in estrogen-related disease. *Trends Pharmacol. Sci.* **2008**, *29*, 116–123.

(9) Filardo, E. J.; Graeber, C. T.; Quinn, J. A.; Resnick, M. B.; Giri, D.; DeLellis, R. A.; Steinhoff, M. M.; Sabo, E. Distribution of GPR30, a seven membrane-spanning estrogen receptor, in primary breast cancer and its association with clinicopathologic determinants of tumor progression. *Clin. Cancer Res.* **2006**, *12*, 6359–6366.

(10) Smith, H. O.; Leslie, K. K.; Singh, M.; Qualls, C. R.; Revankar, C. M.; Joste, N. E.; Prossnitz, E. R. GPR30: a novel indicator of poor survival for endometrial carcinoma. *Am. J. Obstet. Gynecol.* **2007**, *196*, 386.e1–386.e11.

(11) Katzenellenbogen, B. S.; Katzenellenbogen, J. A. Estrogen receptor transcription and transactivation: estrogen receptor alpha and estrogen receptor beta: regulation by selective estrogen receptor modulators and importance in breast cancer. *Breast Cancer Res.* **2000**, *2*, 335–344.

(12) Ariazi, E. A.; Ariazi, J. L.; Cordera, F.; Jordan, V. C. Estrogen receptors as therapeutic targets in breast cancer. *Curr. Top. Med. Chem.* **2006**, *6*, 181–202.

(13) Bologa, C. G.; Revankar, C. M.; Young, S. M.; Edwards, B. S.; Arterburn, J. B.; Kiselyov, A. S.; Parker, M. A.; Tkachenko, S. E.; Savchuck, N. P.; Sklar, L. A.; Oprea, T. I.; Prossnitz, E. R. Virtual and biomolecular screening converge on a selective agonist for GPR30. *Nat. Chem. Biol.* **2006**, *2*, 207–212.

(14) Albanito, L.; Madeo, A.; Lappano, R.; Vivacqua, A.; Rago, V.; Carpino, A.; Oprea, T. I.; Prossnitz, E. R.; Musti, A. M.; Ando, S.; Maggiolini, M. G protein-coupled receptor 30 (GPR30) mediates gene expression changes and growth response to 17β-estradiol and selective GPR30 ligand G-1 in ovarian cancer cells. *Cancer Res.* **2007**, *67*, 1859–1866.

(15) Brailoiu, E.; Dun, S. L.; Brailoiu, G. C.; Mizuo, K.; Sklar, L. A.; Oprea, T. I.; Prossnitz, E. R.; Dun, N. J. Distribution and characterization of estrogen receptor G protein-coupled receptor 30 in the rat central nervous system. *J. Endocrinol.* **2007**, *193*, 311–321.

(16) Pang, Y.; Dong, J.; Thomas, T. Estrogen signaling characteristics of Atlantic Croaker G protein-coupled receptor 30 (GPR30) and evidence it is involved in maintenance of oocyte meiotic arrest. *Endocrinology* **2008**, *149*, 3410–3426.

(17) Albanito, L.; Sisci, D.; Aquila, S.; Brunelli, E.; Vivacqua, A.; Madeo, A.; Lappano, R.; Pandey, D. P.; Picard, D.; Mauro, L.; Ando, S.; Maggiolini, M. Epidermal growth factor induces G protein-coupled receptor 30 expression in estrogen receptor-negative breast cancer cells. *Endocrinology* **2008**, *149*, 3799–3808.

(18) Teng, J.; Wang, Z.-Y.; Prossnitz, E. R.; Bjorling, D. E. The G protein-coupled receptor GPR30 inhibits human urothelial cell proliferation. *Endocrinology* **2008**, *149*, 4024–4034.

(19) Sirianni, R.; Chimento, A.; Ruggiero, C.; Luca, A. D.; Lappano, R.; Ando, S.; Maggiolini, M.; Pezzi, V. The novel estrogen receptor, G protein-coupled receptor 30, mediates the proliferative effects induced by 17β-estradiol on mouse spermatogonial GC-1 cell line. *Endocrinology* **2008**, *149*, 5043–5051.

(20) Wang, C.; Dehghani, B.; Magrisso, I. J.; Rick, E. R.; Bonhomme, E.; Cody, D. B.; Elenich, L. A.; Subramanian, S.; Murphy, S. J.; Kelly, M. J.; Rosenbaum, J. S.; Vandenbark, A. A.; Offner, H. GPR30 contributes to estrogen-induced thymic atrophy. *Mol. Endocrinol.* **2008**, *22*, 636–648.

(21) Madak-Erdogana, Z.; Kieser, K. J.; Kim, S. H.; Komm, B.; Katzenellenbogen, J. A.; Katzenellenbogen, B. S. Nuclear and extranuclear pathway inputs in the regulation of global gene expression by estrogen receptors. *Mol. Endocrinol.* **2008**, *22*, 2116–2127.

(22) Alyea, R. A.; Laurence, S. E.; Kim, S. H.; Katzenallenbogen, B. S.; Katzenallenbogen, J. A.; Watson, C. S. The roles of membrane estrogen receptor subtypes in modulating dopamine transporters in PC-12 cells. *J. Neurochem.* **2008**, *106*, 1525–1533.

(23) Kamanga-Sollo, E.; White, M. E.; Chung, K. Y.; Johnson, B. J.; Dayton, W. R. Potential role of G-protein-coupled receptor 30 (GPR30) in estradiol-17β-stimulated IGF-I mRNA expression in

bovine satellite cell cultures. *Domest. Anim. Endocrinol.* **2008**, *35*, 254–262.

(24) Otto, C.; Rohde-Schulz, B.; Schwarz, G.; Fuchs, I.; Klewer, M.; Brittain, D.; Langer, G.; Bader, B.; Prelle, K.; Nubbemeyer, R.; Fritzemeier, K.-H. G protein-coupled receptor 30 localizes to the endoplasmic reticulum and is not activated by estradiol. *Endocrinology* **2008**, *149*, 4846–4856.

(25) Dun, S. L.; Brailoiu, G. C.; Gao, X.; Brailoiu, E.; Arterburn, J. B.; Prossnitz, E. R.; Oprea, T. I.; Dun, N. J. Expression of estrogen receptor GPR30 in the rat spinal cord, autonomic and sensory ganglia. *J. Neurosci. Res.* **2009**, *87*, 1610–1619.

(26) Dennis, M. K.; Burai, R.; Ramesh, C.; Petrie, W. K.; Alcon, S. N.; Nayak, T. K.; Bologa, C. G.; Leitao, A.; Brailoiu, E.; Deliu, E.; Dun, N. J.; Sklar, L. A.; Hathaway, H. J.; Arterburn, J. B.; Oprea, T. I.; Prossnitz, E. R. In vivo effects of a GPR30 antagonist. *Nat. Chem. Biol.* **2009**, *5*, 421–427.

(27) Hochberg, R. B.; Rosner, W. Interaction of 16 α-[125I]iodo-estradiol with estrogen receptor and other steroid-binding proteins. *Proc. Natl. Acad. Sci. U.S.A.* **1980**, *77*, 328–332.

(28) Katzenellenbogen, J. A.; Carlson, K. E.; Heiman, D. F.; Goswami, R. Receptor-binding radiopharmaceuticals for imaging breast tumors: estrogen-receptor interactions and selectivity of tissue uptake of halogenated estrogen analogs. *J. Nucl. Med.* **1980**, *21*, 550–558.

(29) Cummins, C. H. Radiolabeled steroidal estrogens in cancer research. *Steroids* **1993**, *58*, 245–259.

(30) Hanson, R. N. Synthesis of Auger electron-emitting radiopharmaceuticals. *Curr. Pharm. Des.* **2000**, *6*, 1457–1468.

(31) Van de Wiele, C.; De Vos, F.; Slegers, G.; Van Belle, S.; Dierckx, R. A. Radiolabeled estradiol derivatives in breast cancer: a review. *Eur. J. Nucl. Med.* **2000**, *27*, 1421–1433.

(32) McGuire, A. H.; Dehdashti, F.; Siegel, B. A.; Lyss, A. P.; Brodack, J. W.; Mathias, C. J.; Mintun, M. A.; Katzenellenbogen, J. A.; Welch, M. J. Positron tomographic assessment of 16 α-[18F] fluoro-17β-estradiol uptake in metastatic breast carcinoma. *J. Nucl. Med.* **1991**, *32*, 1526–1531.

(33) Yoshida, Y.; Kurokawa, T.; Sawamura, Y.; Shinagawa, A.; Okazawa, H.; Fujibayashi, Y.; Kotsuji, F. The positron emission tomography with F18 17β-estradiol has the potential to benefit diagnosis and treatment of endometrial cancer. *Gynecol. Oncol.* **2007**, *104*, 764–766.

(34) Yoo, J.; Dence, C. S.; Sharp, T. L.; Katzenellenbogen, J. A.; Welch, M. J. Synthesis of an estrogen receptor β-selective radioligand: 5-[18F]fluoro-(2R*,3S*)-2,3-bis(4-hydroxyphenyl)pentanenitrile and comparison of in vivo distribution with 16α-[18F]fluoro-17β-estradiol. *J. Med. Chem.* **2005**, *48*, 6366–6378.

(35) Linden, H. M.; Stekhova, S. A.; Link, J. M.; Gralow, J. R.; Livingston, R. B.; Ellis, G. K.; Petra, P. H.; Peterson, L. M.; Schubert, E. K.; Dunnwald, L. K.; Krohn, K. A.; Mankoff, D. A. Quantitative fluoroestradiol positron emission tomography imaging predicts response to endocrine treatment in breast cancer. *J. Clin. Oncol.* **2006**, *24*, 2793–2799.

(36) Rijks, L. J. M.; Boer, G. J.; Endert, E.; de Bruin, K.; Janssen, A. G. M.; van Royen, E. A. The Z-isomer of 11β-methoxy-17α-[123I]-iodovinylestradiol is a promising radioligand for estrogen receptor imaging in human breast cancer. *Nucl. Med. Biol.* **1997**, *24*, 65–75.

(37) Fischer, T.; Schomacker, K.; Schicha, H. Diethylstilbestrol (DES) labeled with Auger emitters: potential radiopharmaceutical for therapy of estrogen receptor-positive tumors and their metastases? *Int. J. Radiat. Biol.* **2008**, *84*, 1112–1122.

(38) Kouznetsov, V. V. Recent synthetic developments in a powerful imino Diels−Alder reaction (Povarov reaction): application to the synthesis of *N*-polyheterocycles and related alkaloids. *Tetrahedron* **2009**, *6*, 2721–2750.

(39) Kobayashi, S.; Sugiura, M.; Kitagawa, H.; Lam, W. W.-L. Rare-earth metal triflates in organic synthesis. *Chem. Rev.* **2002**, *102*, 2227–2302.

(40) Moran, D. B.; Morton, G. O.; Albright, J. D. Synthesis of (pyridinyl)-1,2,4-triazolo[4,3-a]pyridines. *J. Heterocycl. Chem.* **1986**, *23*, 1071–1077.

(41) Hanson, R. N.; Napolitano, E.; Fiaschi, R. Synthesis and evaluation of 11β-substituted 21-choloro/iodo-(17α,20E/Z)-19-norpregna-1,3,5(10),20-tetraene-3,17β-diols: high affinity ligands for the estrogen receptor. *J. Med. Chem.* **1998**, *41*, 4686–4692.

(42) Arterburn, J. B.; Rao, K. B.; Perry, M. C. Novel 17α-ethynylestradiol derivatives: Sonogashira couplings using unprotected phenylhydrazines. *Tetrahedron Lett.* **2000**, *41*, 839–842.

(43) Sirisoma, N. S.; Johnson, C. R. α-Iodocycloalkenones: synthesis of (±)- epibatidine. *Tetrahedron Lett.* **1998**, *39*, 2059–2062.

(44) Pimlott, S.; Stevenson, L.; Wyper, D.; Sutherland, A. Rapid and efficient radiosynthesis of [123I]I-PK11195, a single photon emission computed tomography tracer for peripheral benzodiazepine receptors. *Nucl. Med. Biol.* **2008**, *35*, 537–542.

(45) Ramesh, C.; Bryant, B.; Nayak, T.; Revankar, C. M.; Anderson, T.; Carlson, K. E.; Katzenellenbogen, J. A.; Sklar, L. A.; Norenberg, J. P.; Prossnitz, E. R.; Arterburn, J. B. Linkage effects on binding affinity and activation of GPR30 and estrogen receptors ERα/β with tridentate pyridin-2-yl hydrazine tricarbonyl-Re/99mTc(I) chelates. *J. Am. Chem. Soc.* **2006**, *128*, 14476–14477.

(46) Nayak, T. K.; Hathaway, H. J.; Ramesh, C.; Arterburn, J. B.; Dai, D.; Sklar, L. A.; Norenberg, J. P.; Prossnitz, E. R. Preclinical development of a neutral, estrogen receptor-targeted, tridentate 99mTc(I)-estradiol-pyridin-2-yl hydrazine derivative for imaging of breast and endometrial cancers. *J. Nucl. Med.* **2008**, *49*, 978–986.